Universität Zürich[UZH]

Development of an MCMC Method for Studying the Internal Structure of Uranus

Niels FAUCHER

Master Computational Physics - University of Franche-Comté

Summer Internship - University of Zurich

2024

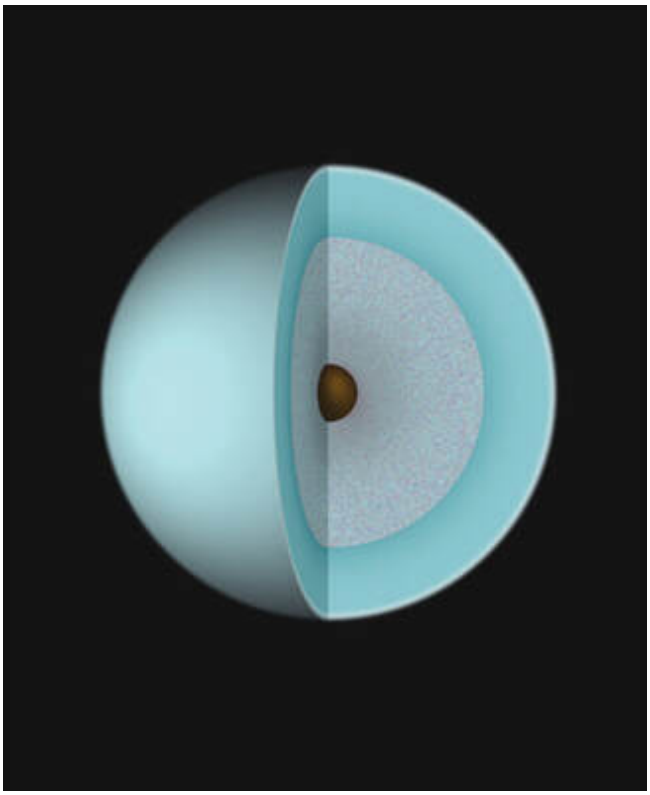

Supervisor :

Ravit HELLED - Saburo HOWARD

Contents

1 Introduction **1**

2 Familiarizing myself with the CEPAM tool **1**
2.1 Installing the Software and Familiarizing Myself with It . . . 1
2.2 Testing Static Models for Uranus . . . 1
2.3 Aim . . . 2

3 Building Our MCMC **3**
3.1 Process Implementation . . . 3
3.1.1 Building the MC and Integrating CEPAM . . . 3
3.1.2 Building the MCMC and Implementing the Bayesian Process . . . 4
3.1.3 Using Multiple Laws of Probability for Efficient Sampling . . . 5
3.1.4 Choosing the Starting Point Randomly . . . 6
3.1.5 Walkers & Iterations . . . 6
3.2 First Phase Analysis . . . 7
3.2.1 Primary Tests . . . 7
3.2.2 Primary Results . . . 8

4 Results **10**
4.1 Planet composed solely of ice - 100% ICE . . . 10
4.1.1 EOS Sesame-Water . . . 11
4.1.2 EOS Reos 4-Mazevet . . . 12
4.2 Planet composed solely of rocks - 100% ROCK . . . 14
4.3 Planet composed of ices and rocks - 50% ICE - 50% ROCK . . . 16

5 Discussion & Conclusion **18**

References **22**

List of Figures

1 Sensibility analysis of parameters . . . 3
2 REQ VS J2 with 100% Ices in Envelope - EOS Sesame . . . 7
3 R_{eq} (km) vs. J_2 $\times 10^6$ - 100% Ices in Envelope - EOS Sesame . . . 8
4 $Z_{1(ICES)}$ vs. $Z_{2(ICES)}$ . . . 9
5 M_{core} (M_U) vs. P_{12}(Mbar) . . . 10
6 Corner Plot - 100% Ices - EOS Sesame_Water . . . 11
7 Corner Plot - 100% Ices - EOS Reos4-Mazevet . . . 12
8 Corner Plot - 100% Rocks - EOS Sesame-drysand . . . 14
9 Corner Plot - 50% Ices 50% Rocks . . . 16
10 Illustration results - 100% Ices for 2 differents EOS - EOS Sesame, EOS Reos4 and EOS Reos3b (HE-H) . . . 18
11 Illustration results - 100% Rocks - 50% Ices 50% Rocks - EOS Sesame-drysand, EOS Reos4 and EOS Reos3b (HE-H) . . . 18
12 Illustration results and pie-chart of the HE-H proportion and Z_1, Z_2 Mass Proportion (Uranus) - 100% Ices) - EOS Sesame and EOS Reos3b (HE-H) . . . 20
13 Illustration results and pie-chart of the HE-H proportion and Z_1, Z_2 Mass Proportion (Uranus) - 100% Ices - EOS Reos4 and EOS Reos3b (HE-H) . . . 20
14 Illustration results and pie-chart of the HE-H proportion and Z_1, Z_2 Mass Proportion (Uranus) - 100% Rocks - EOS Sesame-drysand and EOS Reos3b (HE-H) . . . 21
15 Illustration results and pie-chart of the HE-H proportion and Z_1, Z_2 Mass Proportion (Uranus) - 50% Ices 50% Rocks - EOS Reos4 , EOS Sesame-drysand and EOS Reos3b (HE-H) . . . 21

List of Tables

1 Physical and observational parameters for Uranus. . . . 2

1 Introduction

Studying the internal structures of planets, particularly ice giants like Uranus, is crucial for understanding the formation and evolution of our solar system. Ice giants, such as Uranus and Neptune, formed from the primordial gas of the protoplanetary nebula, which primarily consisted of hydrogen and helium. However, unlike gas giants like Jupiter and Saturn, ice giants are smaller and contain a higher proportion of heavy elements, often in the form of ices and rocks. Therefore, their current internal structure is a complex result of their formation and evolution history.

Despite being less massive, Uranus and Neptune are of significant interest to the scientific community, especially since the discovery of thousands of exoplanets has revealed that "sub-Neptune" type planets are among the most abundant in our galaxy [Winn and Fabrycky, 2015]. Understanding Uranus's internal structure not only helps us demystify our own solar system but also sheds light on the nature of many similar exoplanets.

To date, Uranus and Neptune are the only planets in the solar system that have not been the focus of dedicated missions. Aside from the Voyager 2 flyby, which provided limited data, we have little direct information about these distant worlds. Our knowledge of their internal structures is mainly based on theoretical models. Previous studies, such as those by Nettelmann et al. [2013], Helled et al. [2011] and , have attempted to model the internal structure of Uranus. These models range from the traditional three-layer structure (rocky core, icy mantle, gaseous atmosphere) to more complex models with compositional gradients. Additionally, recent empirical models Neuenschwander and Helled [2022], Neuenschwander et al. [2024], Morf et al. [2024] suggest new perspectives on the ice-rock ratios and the potential differences between Uranus and Neptune. Formation models Valletta and Helled [2020, 2022] and evolution models Vazan and Helled [2020], Scheibe et al. [2019, 2021], as well as *ab initio* simulations that explore the behavior of matter under the extreme conditions of ice giants Soubiran and Militzer [2015], Roy et al. [2024] can provide further insights about the interiors of these planets.

Despite these advances, many questions remain. Is Uranus dominated by ices, or do rocks play a more significant role? What is the exact composition of its atmosphere? Are Uranus and Neptune truly similar, or do they have significant differences in their internal structures? A better understanding of these questions will require both more sophisticated models and, ideally, new dedicated exploration missions.

2 Familiarizing myself with the CEPAM tool

To begin the study of Uranus's internal structure, it was necessary to first become acquainted with the tools and software that would be used throughout the research. One such tool is the code CEPAM (Guillot and Morel [1995]), a specialized software for modeling planetary interiors. The initial phase involved installing CEPAM and running various tests to ensure a solid understanding of its functionality and capabilities.

2.1 Installing the Software and Familiarizing Myself with It

The installation process for CEPAM was straightforward but required specific dependencies, which were duly installed. After setting up the software, initial tests were conducted to understand its core functionalities, particularly focusing on static modeling capabilities.

2.2 Testing Static Models for Uranus

With the software successfully installed, the next step involved testing static models specifically tailored for Uranus. These models are essential for gaining preliminary insights into the planet's internal structure by

adjusting various parameters.

Parameters	**Value**
Mass	8.68×10^{28} g
Temp. 1 bar	77.56×10^{1} K
Mean radius	2.5362×10^{9} cm
Equatorial radius	2.5559×10^{9} cm
Polar radius	2.4973×10^{9} cm
Rotation period	6.206×10^{4} sec
Normalised gravitational moments at 1 bar:	
J_2	0.3511×10^{-2}
Observation uncertainties:	
R_{eq}	0.0004×10^{9} cm
J_2	0.00007×10^{-2}

Table 1: Physical and observational parameters for Uranus.

2.3 Aim

The primary objective of this phase was to fit the planet's equatorial radius (R_{eq}) and the second harmonic coefficient (J_2), both of which are critical observational parameters. To achieve this, the following model parameters were systematically varied:

- $M_{\textbf{core}}$ **(**$M_{\textbf{U}}$**)**: The mass of the core expressed in Uranus masses, which significantly influences the overall density and gravitational profile of Uranus.
- Z_1: The proportion of ices in the atmospheric layer. This parameter affects the density and composition of the outer envelope.
- Z_2: The proportion of ices in the deeper interior. This parameter influences the thermal and compositional structure below the atmosphere.
- P **(Mbar)**: The pressure at the boundary between different layers of Uranus's interior, which is crucial for modeling the transition between the planet's outer and inner regions.

By systematically varying these parameters, the study aimed to investigate how changes in these parameters affect the accuracy of fitting the values of R_{eq} and J_2.

Small variations in these parameters can lead to significant changes in R_{eq} and J_2. For example, increasing the ice fraction in the atmospheric layer (Z_1) or in the deeper interior (Z_2) results in a decrease in the equatorial radius, as expected due to the increase in density. This sensitivity to parameter variations highlights the complexity of finding all possible solutions that fit the observed data accurately.

Therefore, employing a Markov Chain Monte Carlo (MCMC) method is essential for this study. An MCMC allows for extensive exploration of the parameter space, making it possible to identify a range of viable solutions that satisfy the observational constraints on R_{eq} and J_2. This approach is particularly valuable when dealing with multiple parameters and complex dependencies between them, as it systematically explores the parameter space and provides a probabilistic understanding of the model's fit to the data.

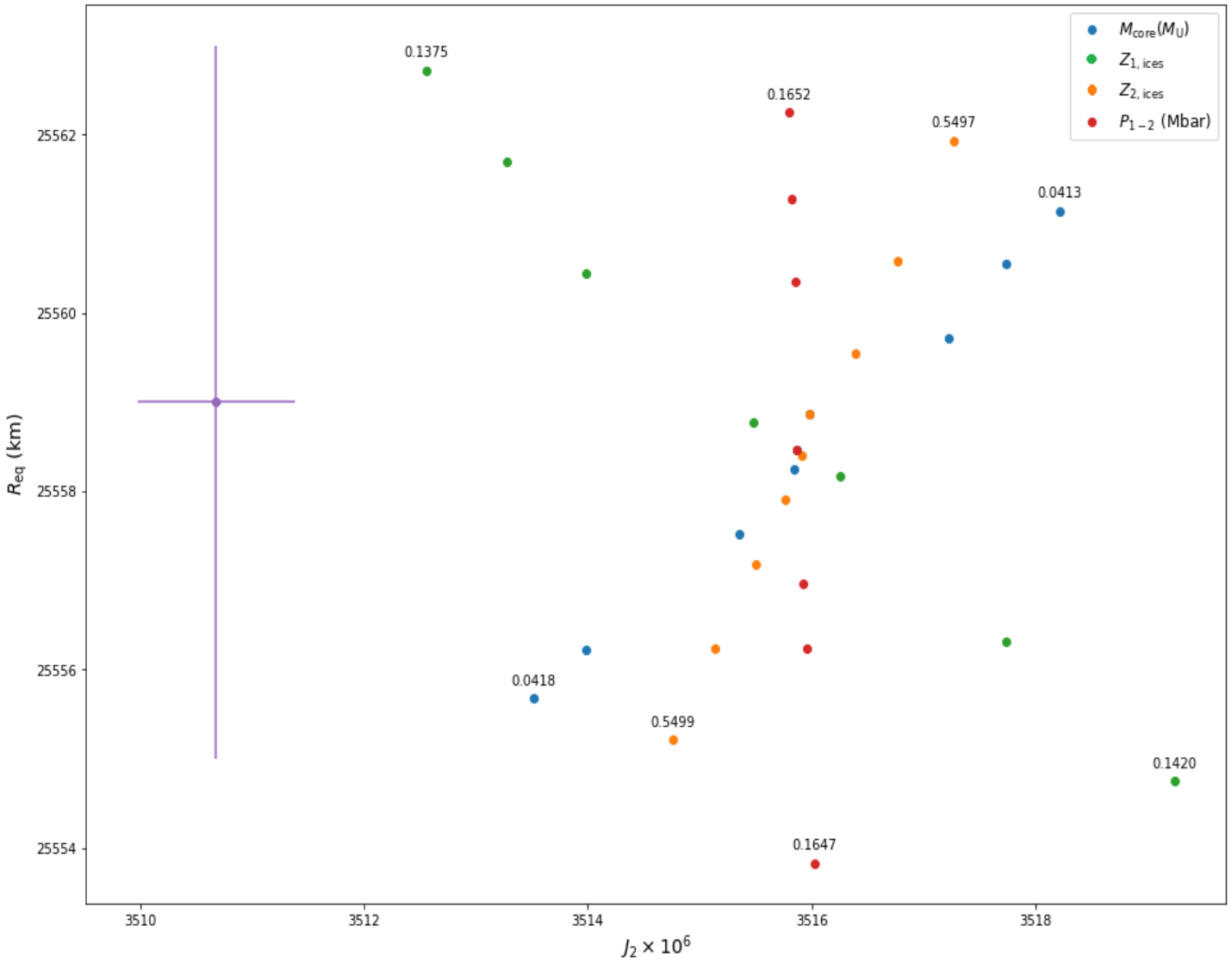

Figure 1: Sensibility analysis of parameters

3 Building Our MCMC

After familiarizing myself with CEPAM and testing static models for Uranus, the next phase of the study involved building the Monte Carlo (MC) and Monte Carlo Markov Chain (MCMC) frameworks to explore the parameter space more efficiently and integrate Bayesian analysis into our model fitting process.

3.1 Process Implementation

3.1.1 Building the MC and Integrating CEPAM

The first step was to construct a basic Monte Carlo (MC) simulation framework. This involved generating random samples from the parameter space and integrating CEPAM into this framework to evaluate the planetary models' outputs based on these random parameters. This integration allowed us to assess how different parameter combinations affected the model's ability to replicate the observed values of R_{eq} and J_2.

3.1.2 Building the MCMC and Implementing the Bayesian Process

With the MC framework established, we extended it using a Monte Carlo Markov Chain (MCMC) approach. MCMC is effective for exploring complex parameter spaces by creating a chain of parameter sets that preferentially sample areas of high likelihood, as informed by Bayesian inference (Bazot et al. [2012]).

Bayesian Inference Overview Bayesian inference combines prior knowledge with observed data to compute the posterior distribution of the parameters. Bayes' theorem is used for this purpose:

$$P(\theta|D) = \frac{P(D|\theta)P(\theta)}{P(D)} \tag{1}$$

where:

- $P(\theta|D)$ is the **posterior** probability of the parameters given the data.
- $P(\theta)$ is the **prior** probability, reflecting our beliefs about the parameters before seeing the data.
- $P(D|\theta)$ is the **likelihood**, showing how likely the observed data is given the parameters.
- $P(D)$ is the **evidence**, representing the total probability of the data across all possible parameters.

Implementing Metropolis-Hastings Algorithm To sample efficiently from the posterior distribution, we used the Metropolis-Hastings algorithm, a popular MCMC method. This algorithm generates a Markov chain that converges to the posterior distribution. Here's how it works:

- A new candidate point θ^* is proposed.
- The acceptance probability ρ is computed as:

$$\rho = \min\left(1, \frac{P(\theta^*|D)}{P(\theta^{(t)}|D)}\right) \tag{2}$$

where $\theta^{(t)}$ is the current point and θ^* is the proposed point. The candidate θ^* is accepted if a random number u (uniformly distributed between 0 and 1) is less than ρ. This process ensures the chain explores the parameter space effectively.

Likelihood Function The likelihood function measures how well the model parameters explain the observed data. Assuming normally distributed errors ϵ_n with variance σ_n^2, and that the errors are independent, the probability density function is:

$$p_\epsilon(\epsilon) = \prod_{n=1}^{N} \frac{1}{\sqrt{2\pi\sigma_n^2}} \exp\left(-\frac{\epsilon_n^2}{2\sigma_n^2}\right) \tag{3}$$

where $\epsilon_n = X_n - S(\theta)$ is the difference between observed data X_n and the model prediction $S(\theta)$. The likelihood function is:

$$L(\theta; X) = \prod_{n=1}^{N} \frac{1}{\sqrt{2\pi\sigma_n^2}} \exp\left(-\frac{1}{2}\sum_{n=1}^{N}\left(\frac{S_n(\theta) - X_n}{\sigma_n}\right)^2\right) \tag{4}$$

3.1.3 Using Multiple Laws of Probability for Efficient Sampling

To optimize the effectiveness of the Markov Chain Monte Carlo (MCMC) algorithm in exploring the parameter space, we implemented a variety of probability distributions to enable both large and small jumps for the walker, the hypothetical particle navigating the parameter space. This approach enhanced sampling efficiency by balancing exploration and exploitation, allowing the algorithm to escape local minima while thoroughly exploring high-probability regions.

However, the more complex aspect of this method lies in empirically determining the weight assigned to these instrumental distributions and the standard deviations of our normal distributions. We employed one uniform distribution and two normal distributions, each serving different purposes: one with a large standard deviation for large jumps and another with a small standard deviation for finer, more localized movements. As previously mentioned, the importance assigned to these distributions is crucial and also depends on our initial conditions.

If the initial conditions are close to the desired values, it is more effective to prioritize small jumps over the uniform distribution or large jumps, as fine-tuning around high-probability areas becomes more critical. Conversely, if starting from random initial conditions, as in our case, careful consideration must be given to the proportion of jumps from each distribution.

Our implementation strategy is as follows:

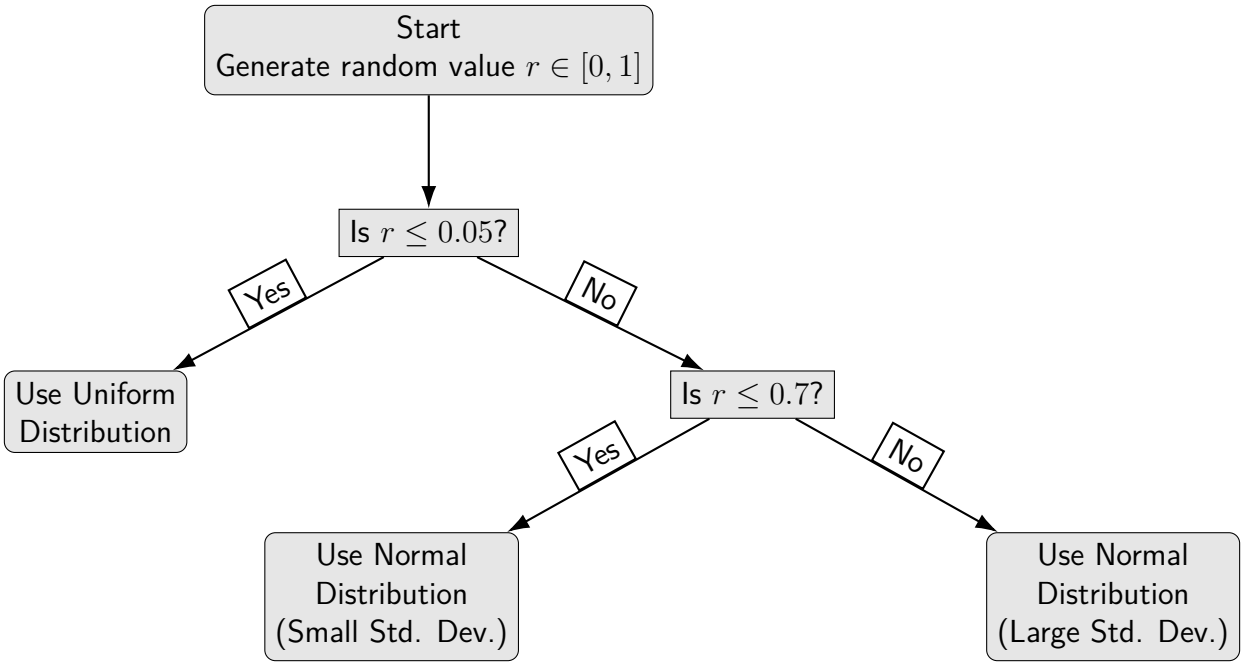

In the scheme, we start by generating a random value between 0 and 1. The value then determines which probability distribution to use for the next step:

- There is a 5% chance of selecting the uniform distribution, which allows for broad exploration.
- A 65% chance of selecting the normal distribution with a small standard deviation, facilitating smaller jumps for more precise exploration.
- A 30% chance of selecting the normal distribution with a large standard deviation, enabling larger jumps for exploring more widely.

This process is done for every parameters and this probabilistic approach ensures a balanced exploration of the parameter space, combining both large-scale exploration and detailed refinement based on the algorithm's needs.

3.1.4 Choosing the Starting Point Randomly

The starting point for each walker in the MCMC was chosen randomly within the defined parameter space. This randomness in initialization helped avoid biasing the results toward any particular region of the parameter space and ensured a more comprehensive exploration of potential solutions.

3.1.5 Walkers & Iterations

After implementing these adjustments and testing the algorithm, we found that a single walker was insufficient for achieving accurate results. By increasing the number of walkers and iterations, the algorithm could explore the parameter space more effectively, improving the reliability of the results.

In Section 4, we used approximately 10 walkers per run. While this may not be the optimal number, it was the best we could manage given our constraints on time and resources. Ideally, using more walkers and iterations would allow for a more thorough exploration of the parameter space, leading to even more accurate results.

3.2 First Phase Analysis

3.2.1 Primary Tests

Figure 3 illustrates the parameter space explored by our MCMC algorithm, differentiating between the models that were accepted and those that were rejected. This plot demonstrates a key aspect of our MCMC approach: it effectively traverses a vast parameter space while selectively accepting only those models that align with our criteria, thereby confirming its robustness and accuracy.

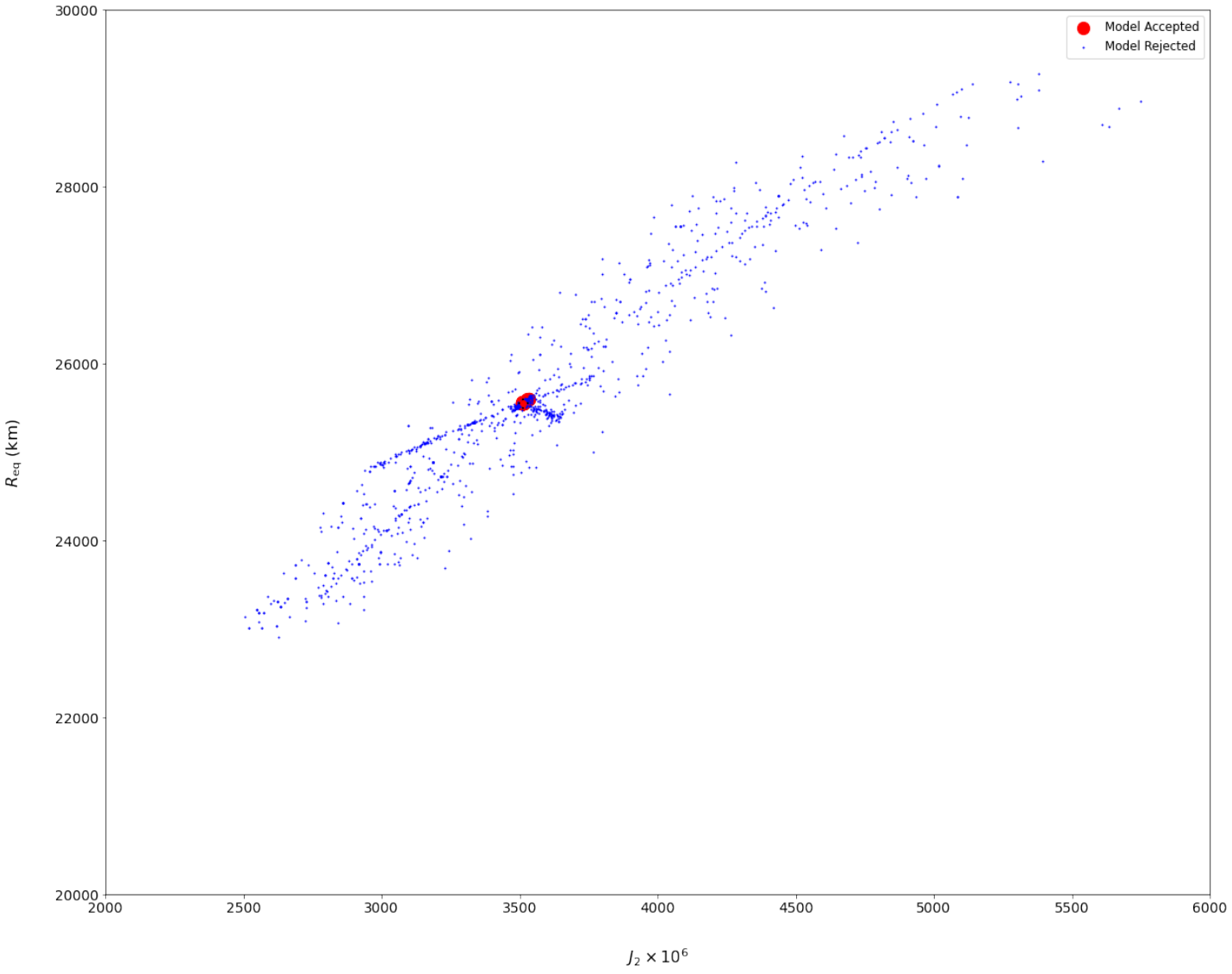

Figure 2: REQ VS J2 with 100% Ices in Envelope - EOS Sesame

3.2.2 Primary Results

The next three figures provide further insights into our results. In the first figure, we see that our walker successfully converges to the correct value and begins sampling appropriately once it reaches the vicinity of this value. The following two figures offer a preliminary view of our final results. Specifically, we are interested in the potential composition of the planet Uranus. It appears that most models suggest the percentage of ice in the atmosphere is between 30% and 50%, with a more precise range of 90% to 92% in the deeper layers. Figure 5 indicates that the core's mass (in units of Uranus' mass) fluctuates between 1.5% and 5.5%, while the pressure at the transition between the outer and inner envelopes ranges from 12.5% to 28%. These findings provide an initial glimpse of what we can expect from our models.

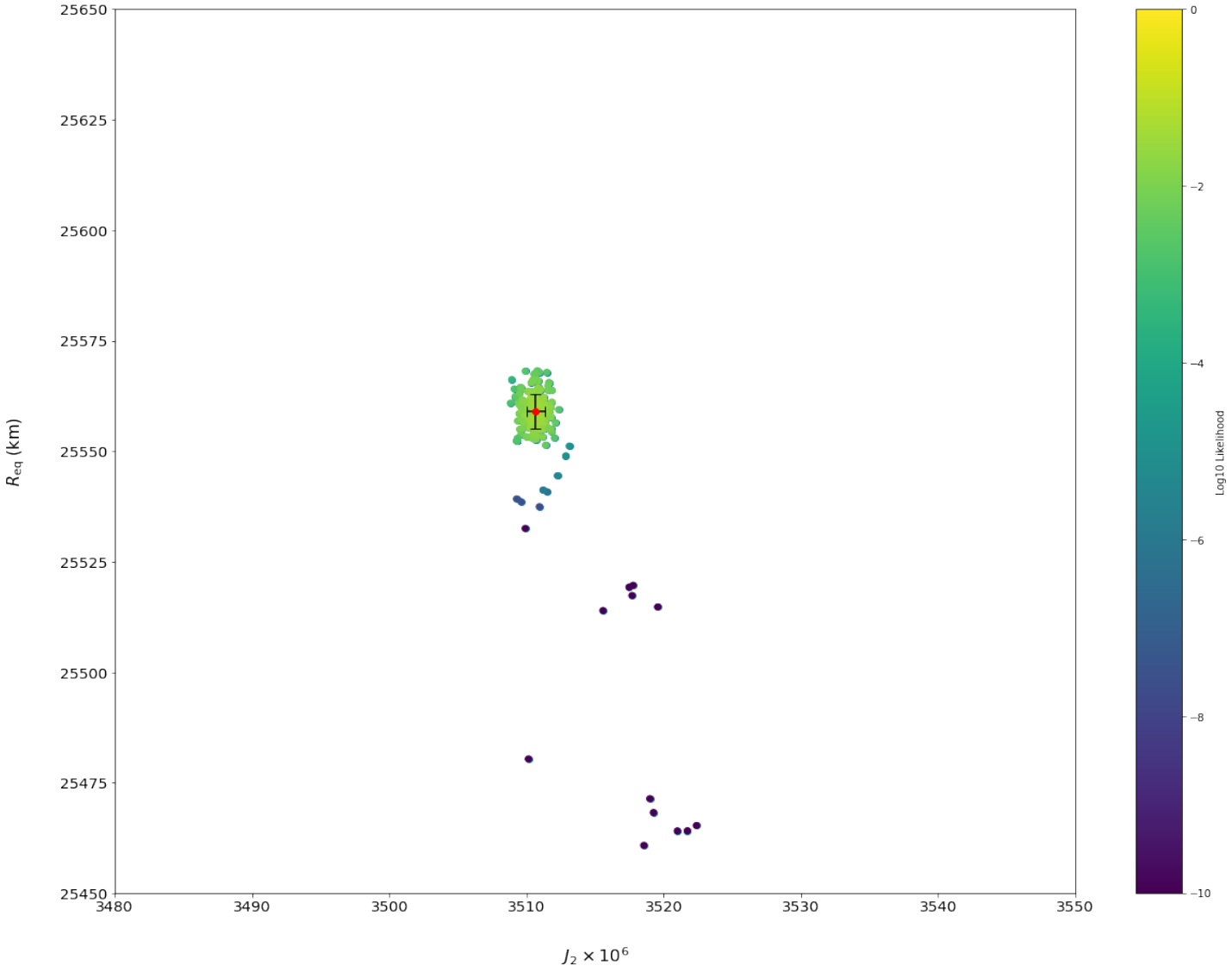

Figure 3: R_{eq} (km) vs. $J_2 \times 10^6$ - 100% Ices in Envelope - EOS Sesame

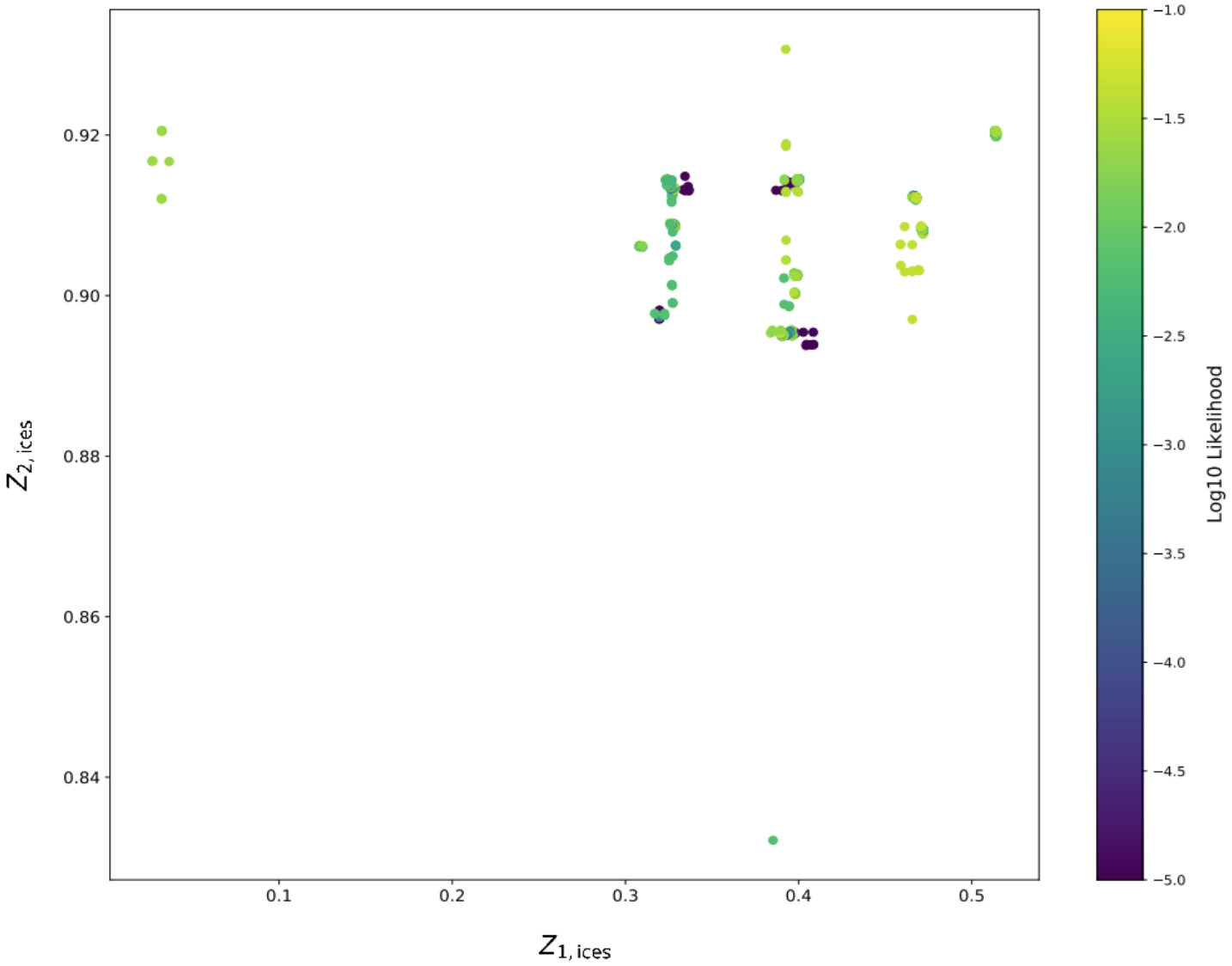

Figure 4: $Z_{1(ICES)}$ vs. $Z_{2(ICES)}$

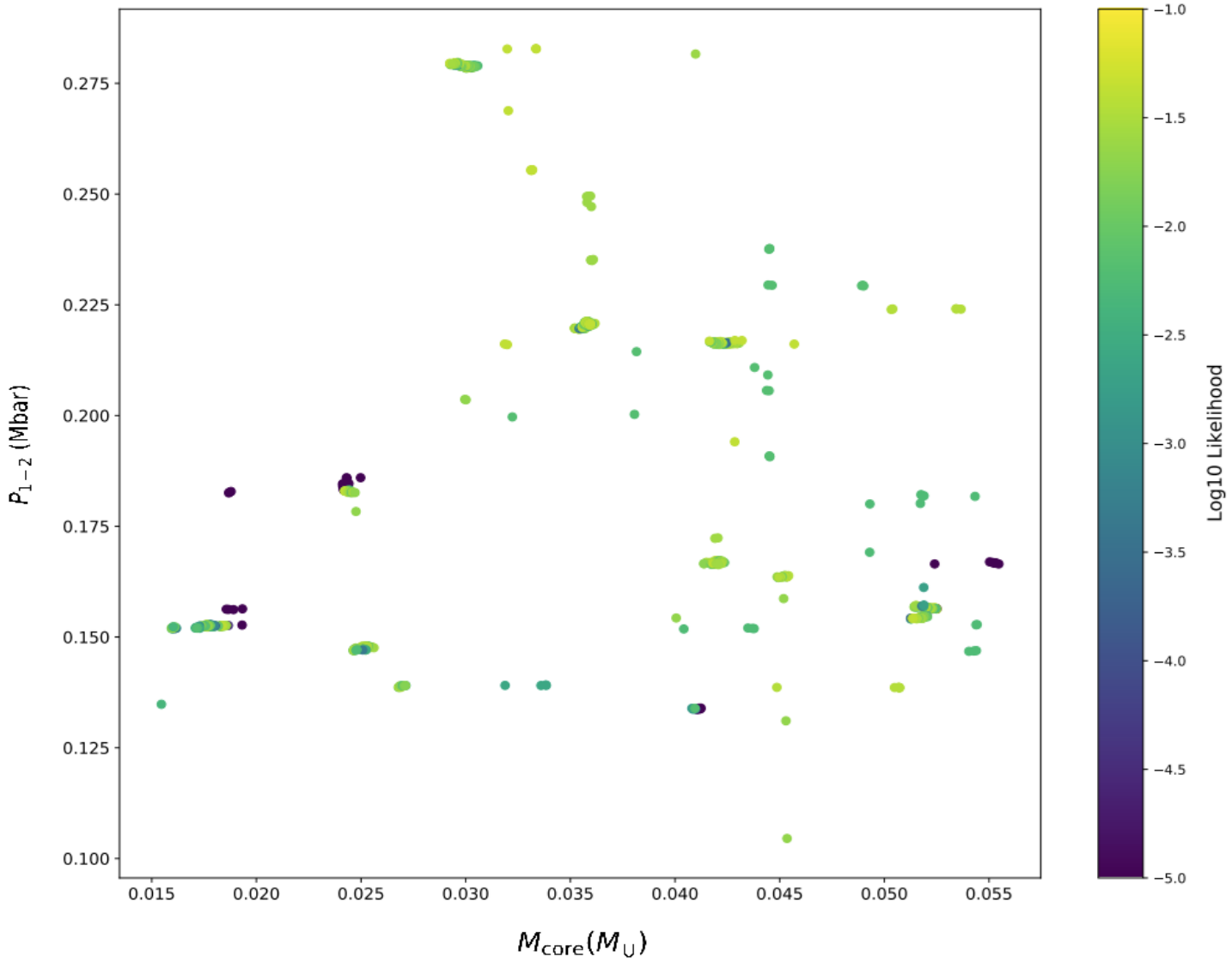

Figure 5: M_{core} (M_U) vs. P_{12}(Mbar)

4 Results

In the following section, we will present our results and discuss them. To obtain a comprehensive set of models, we decided to test different fractions of ice and rock for Uranus's composition. We remind that we used the same amount of walkers per simulation.

4.1 Planet composed solely of ice - 100% ICE

We begin with a model of the planet composed entirely of ice. We have used different equations of state (EOS) in our analysis.

4.1.1 EOS Sesame-Water

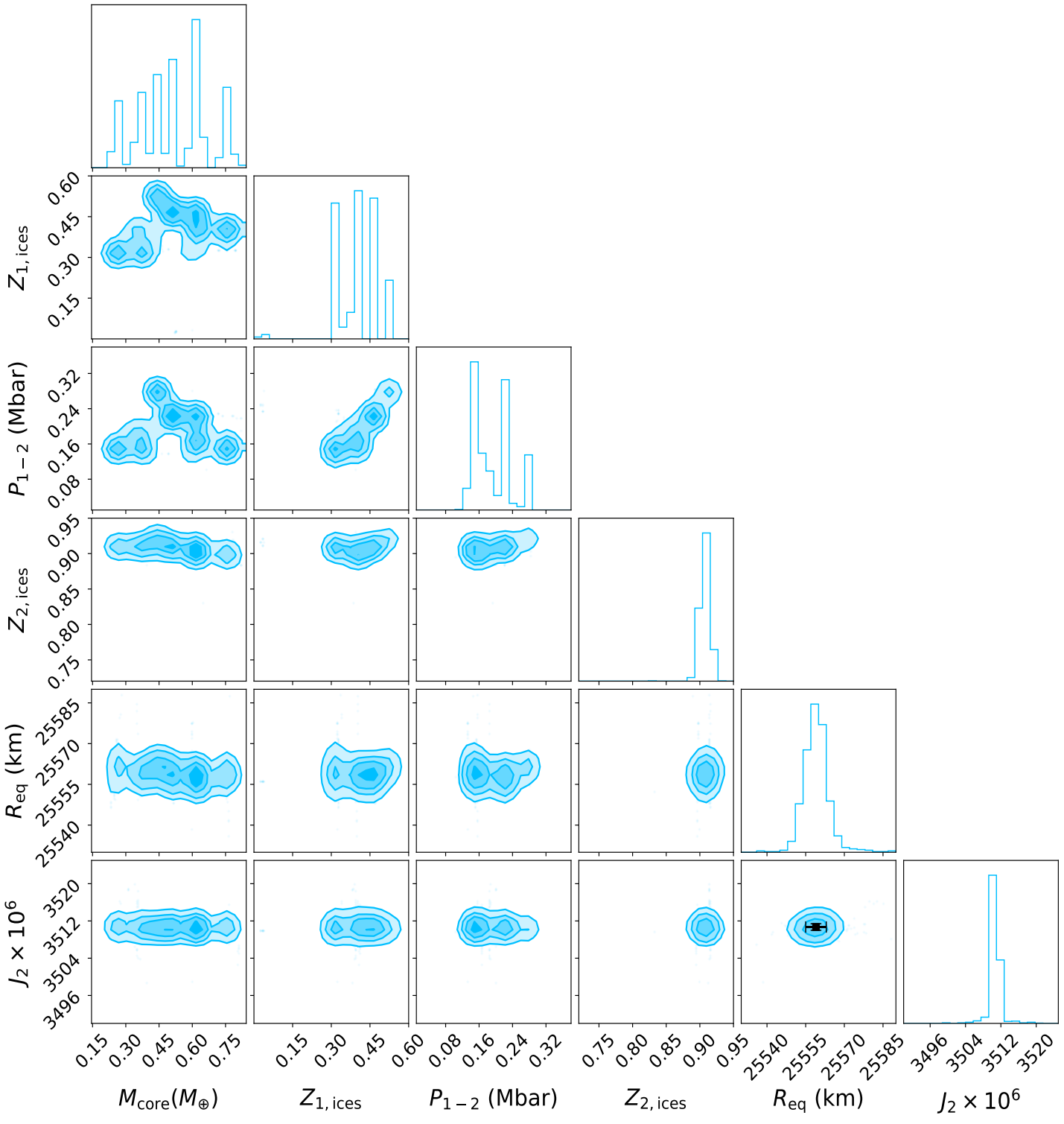

Figure 6: Corner Plot - 100% Ices - EOS Sesame_Water

4.1.2 EOS Reos 4-Mazevet

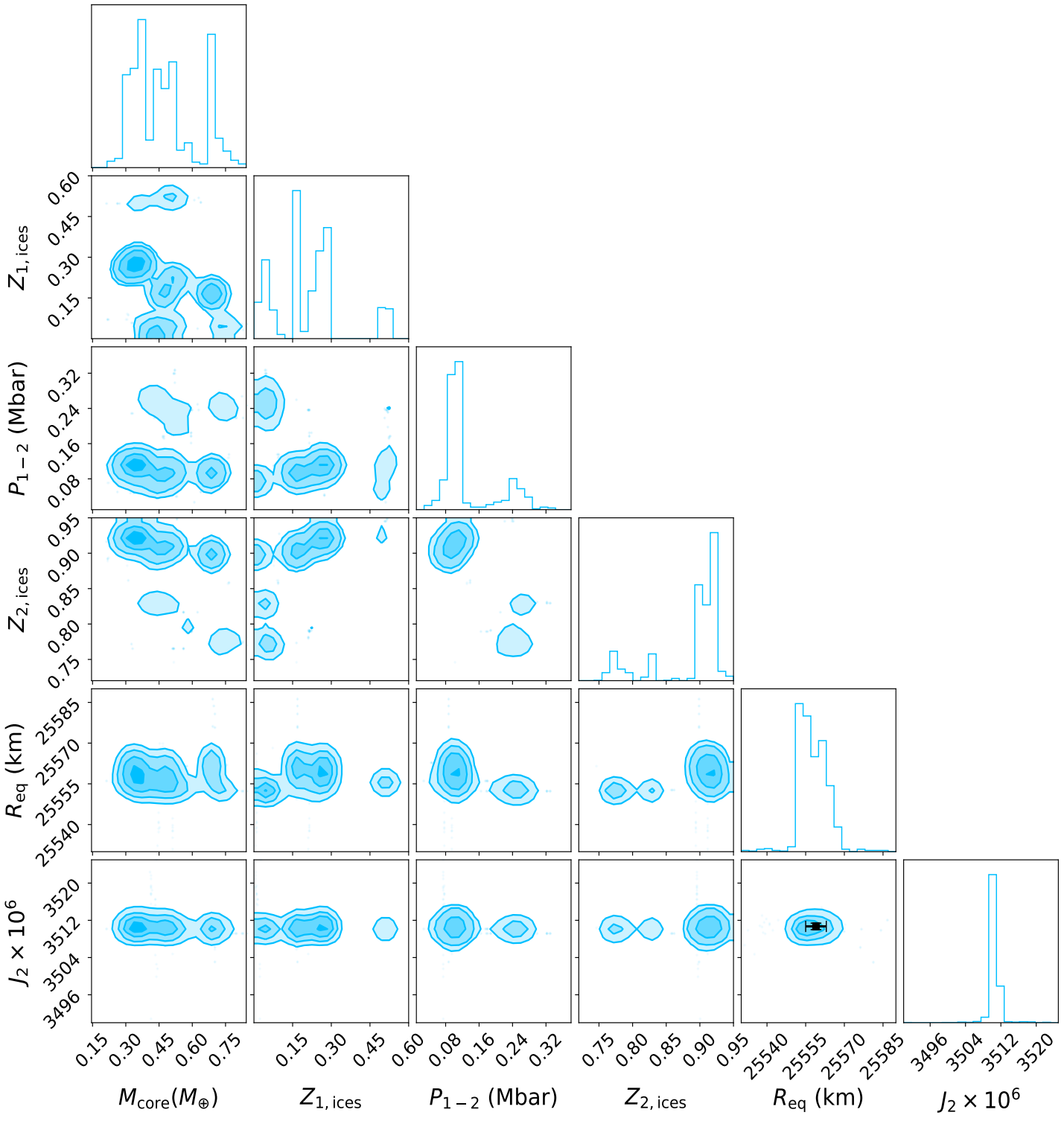

Figure 7: Corner Plot - 100% Ices - EOS Reos4-Mazevet

We observe a clear difference between these two corner plots, highlighting the importance of these equations of state (EOS) in the study of interior models. The mass of the core is roughly the same in both cases. For Z_1, we have a narrower range with the SESAME-water model, where the MCMC method only finds viable models between 25% and 55% of ice. In contrast, for REOS4, it identifies more models between 5% and 30%, suggesting a possible change in Z_2 as well. This is indeed the case with REOS4, where we see a wider interval, allowing for inner part compositions up to 75%, while SESAME-water restricts this range to between 90% and 92%.

Furthermore, we observe a similar behavior for phase separation pressure: with REOS4, more viable models are found between approximately 0.05 and 0.16 Mbar, whereas with SESAME-water, they do not exceed 0.1 Mbar. It is important to note that we provided intervals to the MCMC to guide its search within specific ranges. Additionally, it should be noted that there are instances where we observe clusters of viable models at the boundaries of these intervals. This could provide further insights, such as the need to extend our intervals to explore other possible models.

4.2 Planet composed solely of rocks - 100% ROCK

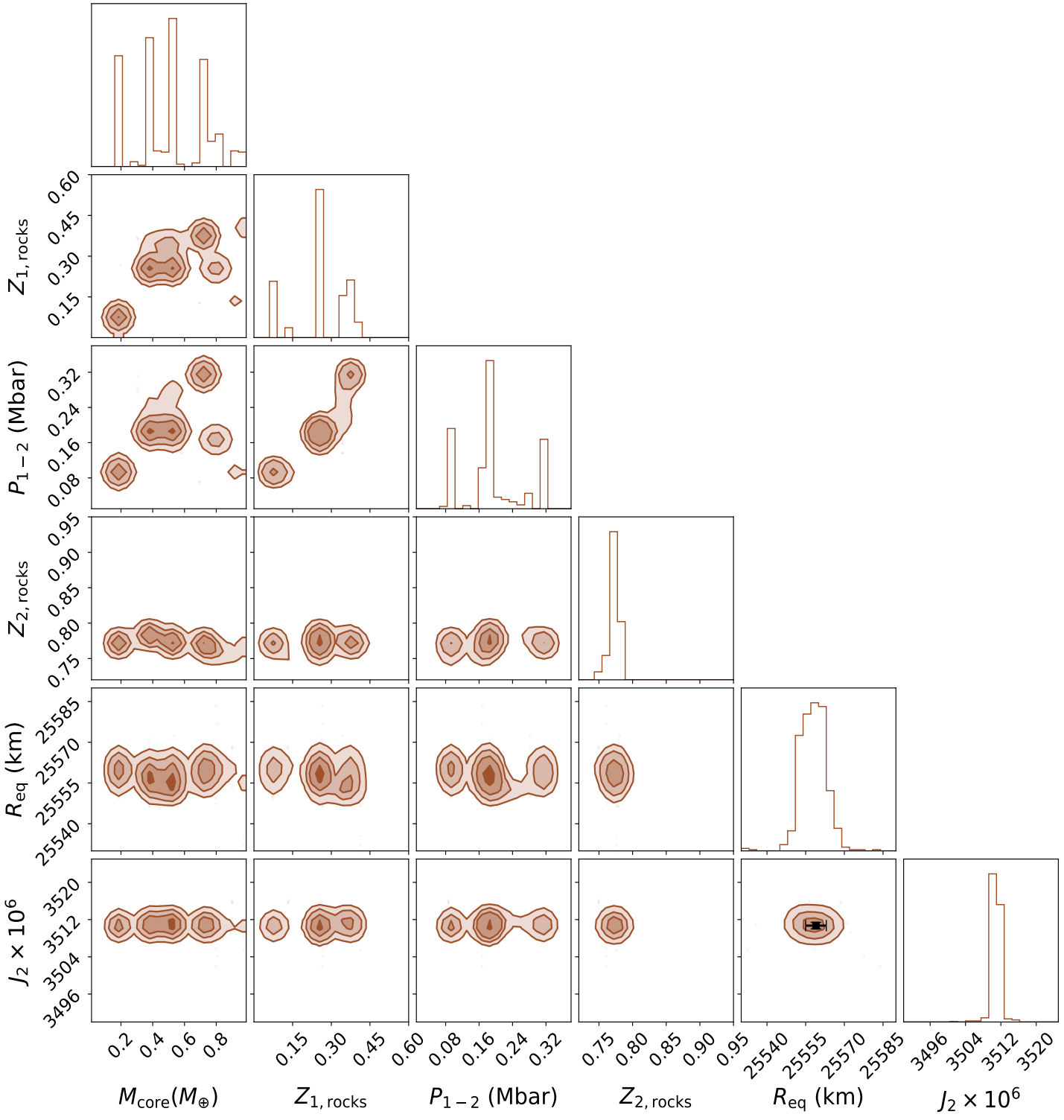

Figure 8: Corner Plot - 100% Rocks - EOS Sesame-drysand

In the case of a planet made entirely of rock, the percentage of rocks in the outer and inner layers is lower compared to ices, which makes sense due to the higher density of rock. Regarding the mass of the core, there is also an increase in the range, from about 10% to approximately 85% of Earth's mass, indicating that we are still considering a relatively small core. For Z_1, the values range between about 5% and 45%, while for Z_2, it is very localized around 77%. Again we were expecting these differences as we explained it before.With this first results in mind we could expect that the composition of 50% ice and 50% rock should be the mean value of the two previous simulation.

4.3 Planet composed of ices and rocks - 50% ICE - 50% ROCK

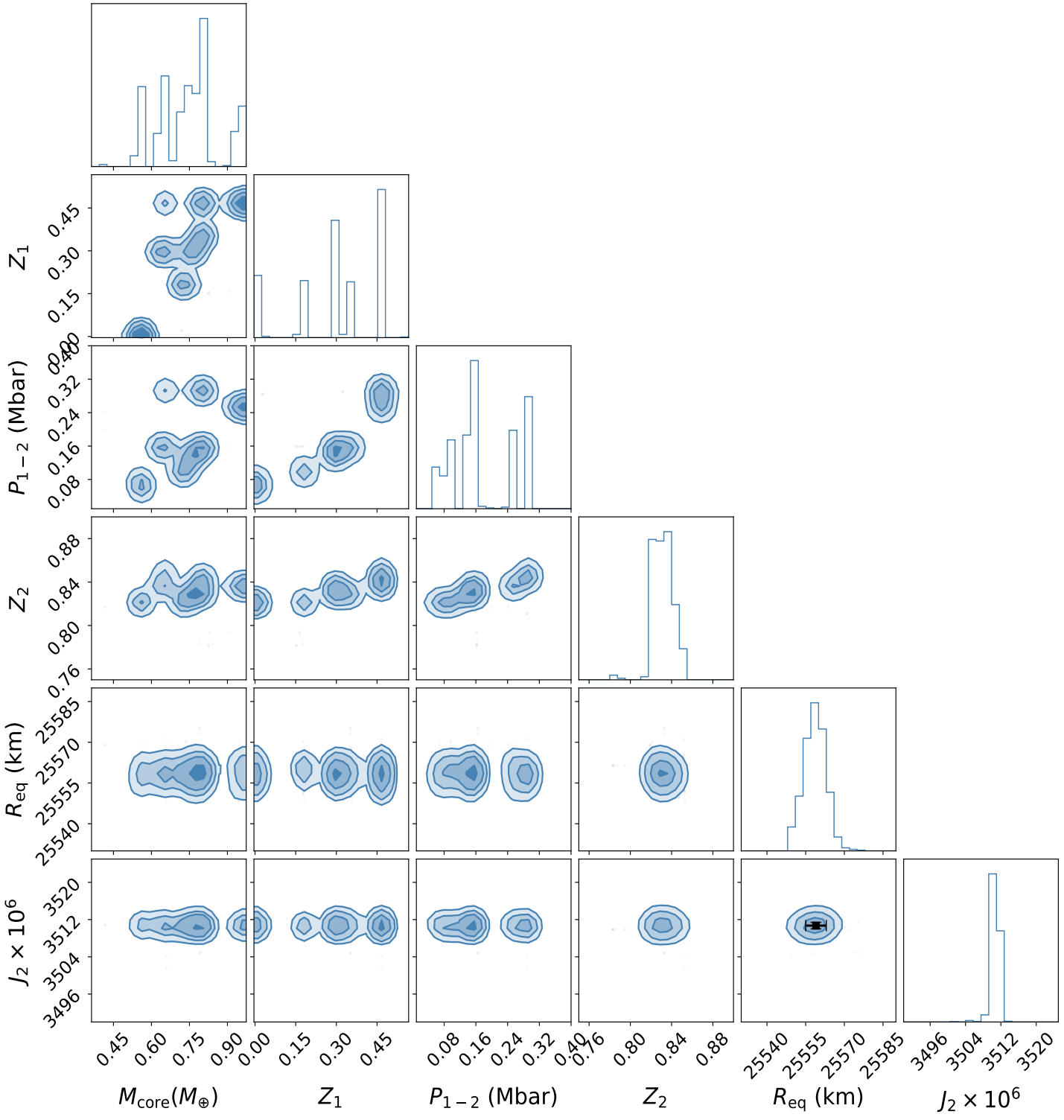

Figure 9: Corner Plot - 50% Ices 50% Rocks

We can now compare the latest results to the previous ones. In this section, we aimed to vary the proportions of rocks and ices simultaneously and by equal amounts. This allows us to check if our initial assumptions were correct regarding the mean value of this plot based on the two previous cases we tested (100% ices and 100% rocks).

For the interval of Z_1, it appears that the current range is broader than we expected, extending from 1% to 50%. This suggests that the outer part should consist of about 25% ice and an equal amount of rock. For Z_2, the range is more as anticipated, between 81% and 86%, falling between the previous ranges. The core mass seems to be larger in this case, with a lower bound of around 50% and an upper bound close to one Earth mass. Finally, for the pressure of phase separation, it appears to be consistent with the value found in the 100% ice simulation.

5 Discussion & Conclusion

In the following section, various illustrations and plots will be discussed, with the results generated using several equations of state (EOS). These include EOS Sesame-Water [Lyon and Johnson, 1992], EOS Reos4-Mazevet [Mazevet et al., 2019], EOS Sesame-Drysand [Lyon and Johnson, 1992].

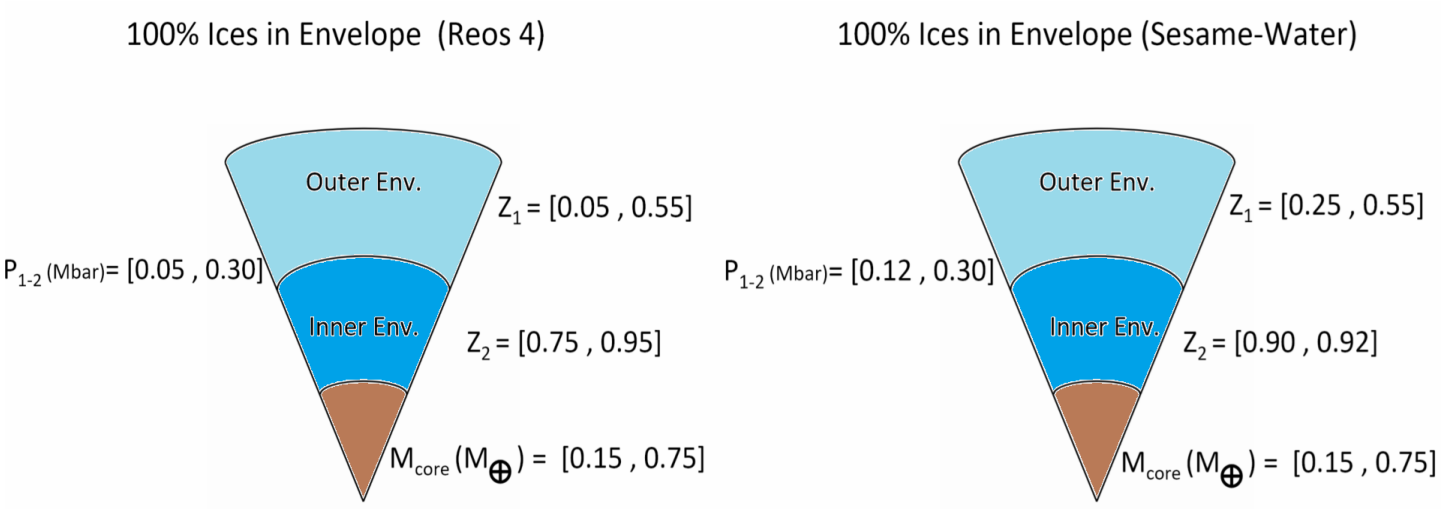

Figure 10: Illustration results - 100% Ices for 2 differents EOS - EOS Sesame, EOS Reos4 and EOS Reos3b (HE-H)

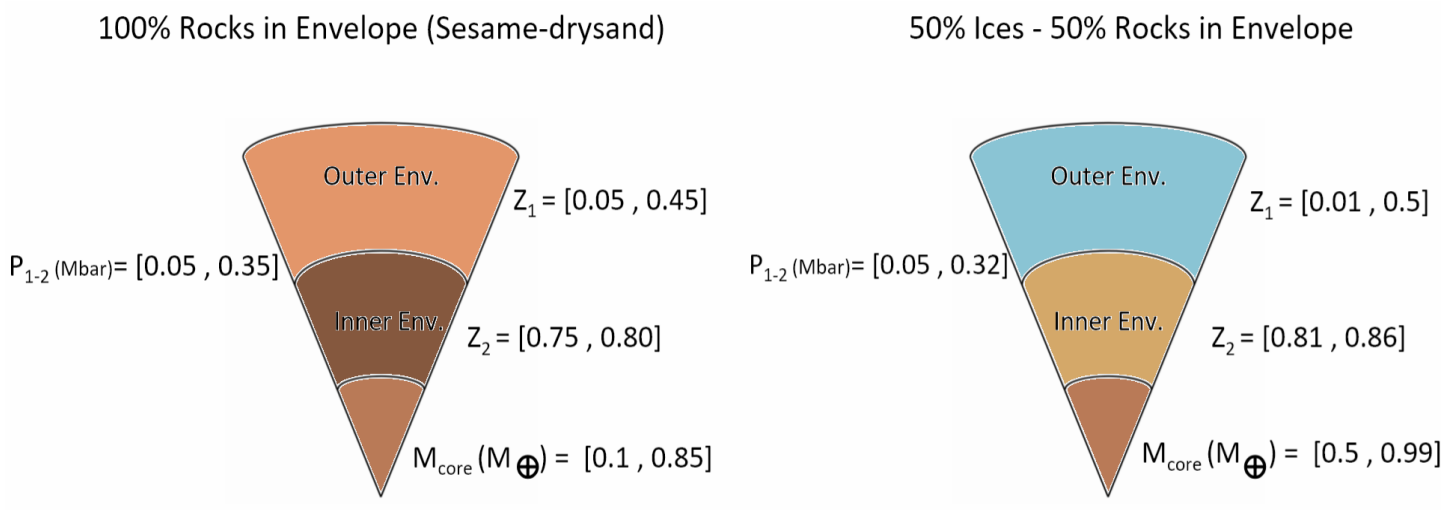

Figure 11: Illustration results - 100% Rocks - 50% Ices 50% Rocks - EOS Sesame-drysand, EOS Reos4 and EOS Reos3b (HE-H)

Based on our previous results, as well as those presented in the Appendix, it appears that the outer part of Uranus is composed of approximately 50% heavy elements and 50% hydrogen-helium (He-H) mixture. In the planet's inner regions, the proportion of He-H can vary significantly, ranging from about 5% to 25%. This variation suggests a complex internal composition for Uranus. Regarding the core, while it is generally believed to be less massive than Earth's, some models suggest it could exceed this mass, warranting further investigation. Additionally, the maximum pressure at which phase separation of the elements occurs is estimated to be around 0.32 Mbar, although the lower limit for this pressure remains uncertain.

In the Appendix, we present similar illustrations to Figures 10 and 11, but these are depicted in terms of mass proportions, including the proportion of He-H. Figures 12 to 15 show that the He-H proportion is around 23% across most simulations, except for those using the Sesame-water equation of state (EOS). When using a newer EOS like REOS4-Mazevet, the He-H proportion appears similar between simulations with 100% rock and 100% ice compositions, as well as for other mixtures. Notably, the total amount of rock and ice also appears similar across these models, though, as mentioned earlier, the distribution changes between the outer and inner parts of the planet. In Figure 15 (with half ices and half rocks in the envelope), the combined mass of rock and ice appears slightly larger than in previous models, totaling almost 80%, with around 20% He-H, which is less than in the earlier models.

To enhance and expand our research, future work could involve exploring a broader range of compositional percentages by widening the intervals used in our models. Allowing these percentages to vary more freely could provide new insights, but this approach would require a more robust Markov Chain Monte Carlo (MCMC) method with additional iterations and more walkers to ensure statistical reliability. Including the gravitational coefficient J_4 in our analysis could also help better constrain the parameter space and improve our understanding of Uranus's internal structure.

Further studies could consider varying the temperature at the 1-bar pressure level (T1bar), exploring different ice-to-rock ratios, and examining alternative structural models. Investigating whether Uranus requires a distinct core or can be better described by a two-layer structure with compositional gradients could provide valuable insights into the planet's formation and evolution. Comparing these findings with data from Neptune, which shares similarities with Uranus but also exhibits notable differences, could offer a comparative perspective that further refines our models and deepens our understanding of ice giant interiors.

By exploring these additional avenues, we can continue to build a more comprehensive picture of Uranus and its place among the giant planets, both within our solar system and beyond.

Appendix

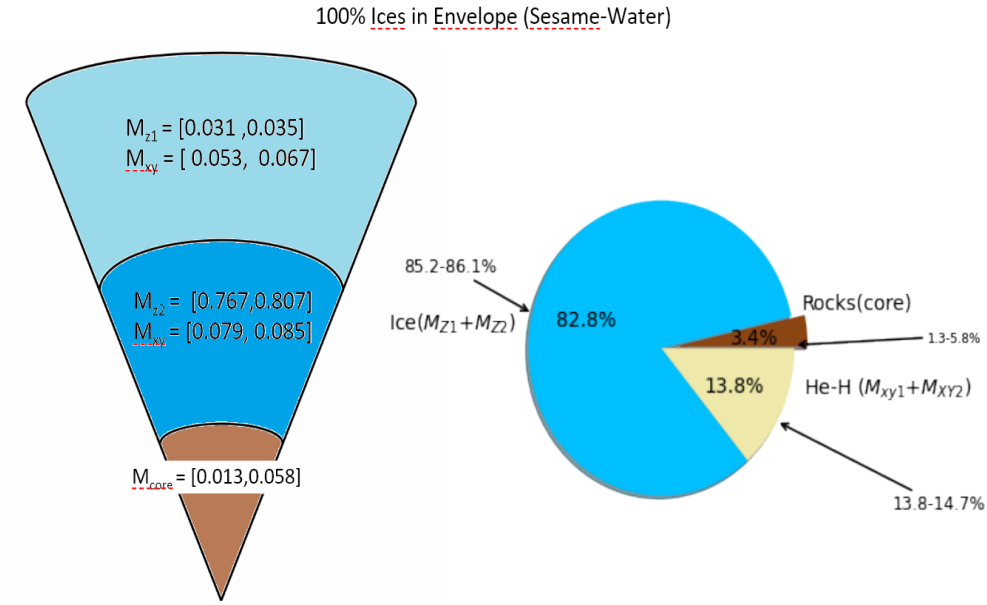

Figure 12: Illustration results and pie-chart of the HE-H proportion and Z_1, Z_2 Mass Proportion (Uranus) - 100% Ices) - EOS Sesame and EOS Reos3b (HE-H)

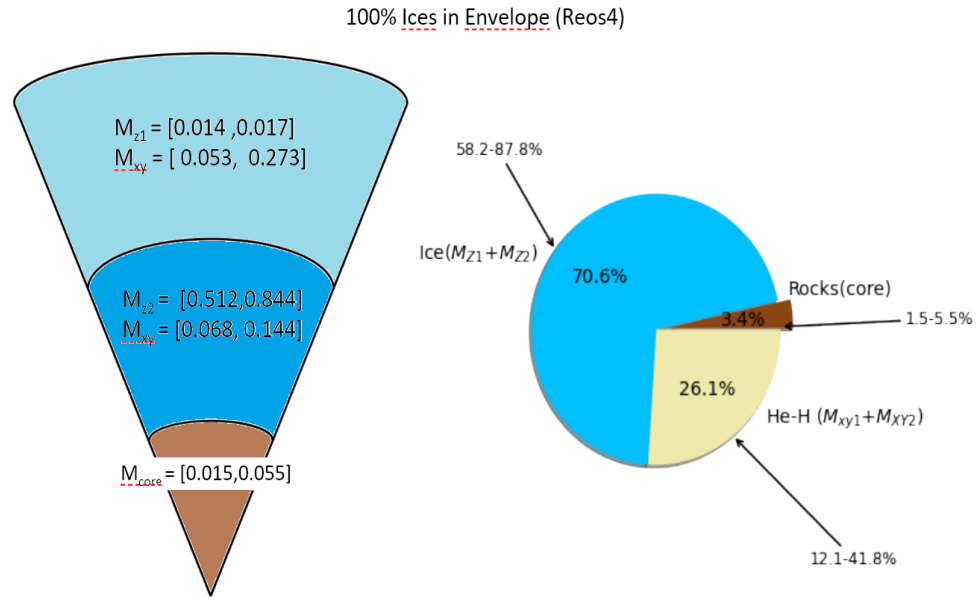

Figure 13: Illustration results and pie-chart of the HE-H proportion and Z_1, Z_2 Mass Proportion (Uranus) - 100% Ices - EOS Reos4 and EOS Reos3b (HE-H)

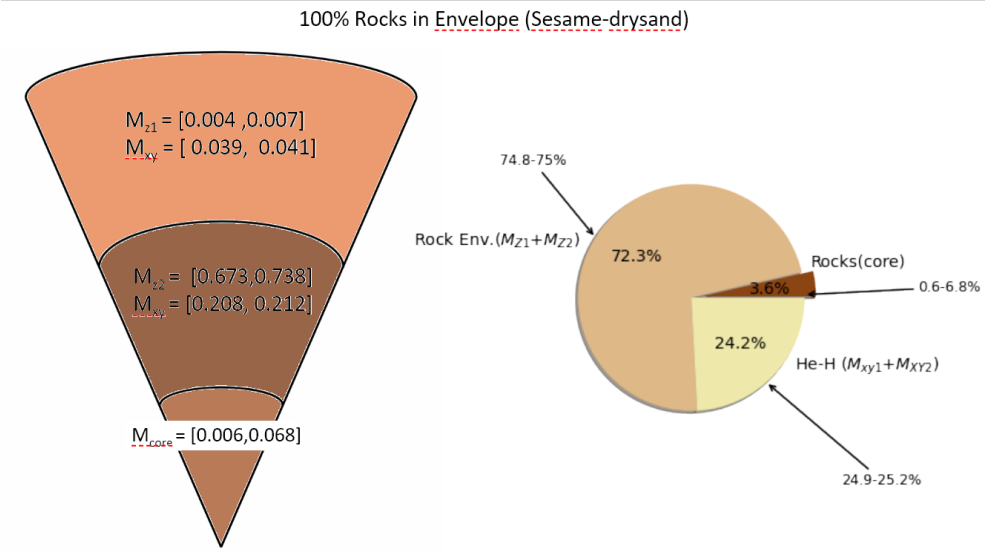

Figure 14: Illustration results and pie-chart of the HE-H proportion and Z_1, Z_2 Mass Proportion (Uranus) - 100% Rocks - EOS Sesame-drysand and EOS Reos3b (HE-H)

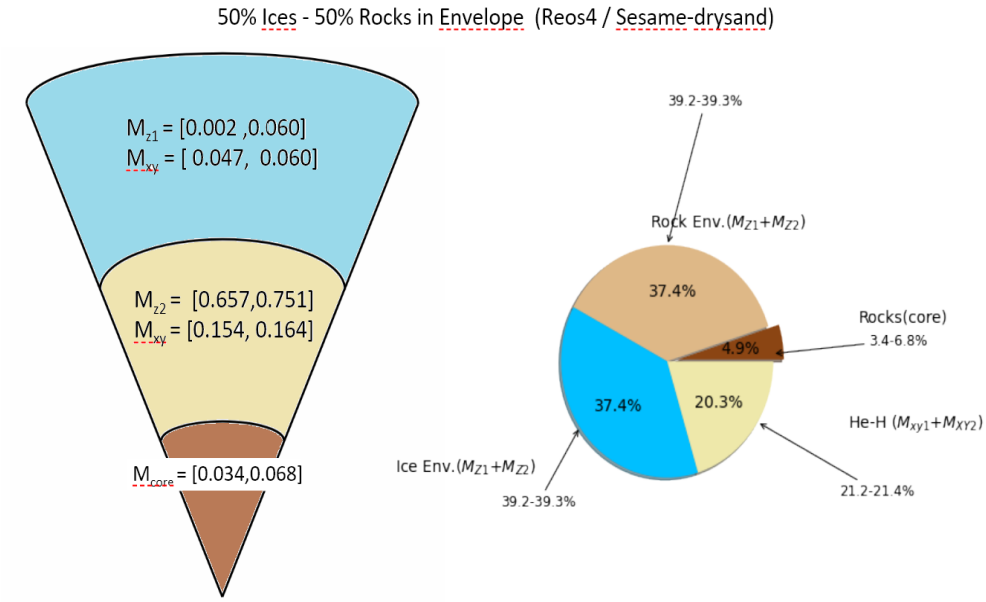

Figure 15: Illustration results and pie-chart of the HE-H proportion and Z_1, Z_2 Mass Proportion (Uranus) - 50% Ices 50% Rocks - EOS Reos4 , EOS Sesame-drysand and EOS Reos3b (HE-H)

References

M. Bazot, S. Bourguignon, and J. Christensen-Dalsgaard. A Bayesian approach to the modelling of alpha Cen A. *Mon. Not. Roy. Astron. Soc.*, 427:1847, 2012. doi: 10.1111/j.1365-2966.2012.21818.x.

T. Guillot and P. Morel. CEPAM: a code for modeling the interiors of giant planets. , 109:109–123, January 1995.

Ravit Helled, John D. Anderson, Morris Podolak, and Gerald Schubert. Interior Models of Uranus and Neptune. , 726(1):15, January 2011. doi: 10.1088/0004-637X/726/1/15.

S. P. Lyon and J. D. Johnson. SESAME: The Los Alamos national laboratory equation of state database. *LANL Report*, LA-UR-92-3407, 1992.

S. Mazevet, A. Licari, G. Chabrier, and A. Y. Potekhin. Ab initio based equation of state of dense water for planetary and exoplanetary modeling. , 621:A128, January 2019. doi: 10.1051/0004-6361/201833963.

Luca Morf, Simon Müller, and Ravit Helled. The interior of Uranus: Thermal profile, bulk composition and the distribution of rock, water and hydrogen and helium. *arXiv e-prints*, art. arXiv:2408.10336, August 2024. doi: 10.48550/arXiv.2408.10336.

N. Nettelmann, R. Helled, J. J. Fortney, and R. Redmer. New indication for a dichotomy in the interior structure of Uranus and Neptune from the application of modified shape and rotation data. , 77:143–151, March 2013. doi: 10.1016/j.pss.2012.06.019.

Benno A. Neuenschwander and Ravit Helled. Empirical structure models of Uranus and Neptune. , 512(3): 3124–3136, May 2022. doi: 10.1093/mnras/stac628.

Benno A. Neuenschwander, Simon Müller, and Ravit Helled. Uranus' complex internal structure. 2024. URL `https://arxiv.org/abs/2401.11769`.

Argha Jyoti Roy, Armin Bergermann, Mandy Bethkenhagen, and Ronald Redmer. Mixture of hydrogen and methane under planetary interior conditions. *Physical Chemistry Chemical Physics (Incorporating Faraday Transactions)*, 26(19):14374–14383, May 2024. doi: 10.1039/D4CP00058G.

Ludwig Scheibe, Nadine Nettelmann, and Ronald Redmer. Thermal evolution of Uranus and Neptune. I. Adiabatic models. , 632:A70, December 2019. doi: 10.1051/0004-6361/201936378.

Ludwig Scheibe, Nadine Nettelmann, and Ronald Redmer. Thermal evolution of Uranus and Neptune. II. Deep thermal boundary layer. , 650:A200, June 2021. doi: 10.1051/0004-6361/202140663.

F. Soubiran and B. Militzer. Hydrogen-water mixtures in giant planet interiors studied with ab initio simulations. *High Energy Density Physics*, 17:157–161, December 2015. doi: 10.1016/j.hedp.2014.10.005.

Claudio Valletta and Ravit Helled. Giant Planet Formation Models with a Self-consistent Treatment of the Heavy Elements. , 900(2):133, September 2020. doi: 10.3847/1538-4357/aba904.

Claudio Valletta and Ravit Helled. Possible In Situ Formation of Uranus and Neptune via Pebble Accretion. , 931(1):21, May 2022. doi: 10.3847/1538-4357/ac5f52.

Allona Vazan and Ravit Helled. Explaining the low luminosity of Uranus: a self-consistent thermal and structural evolution. , 633:A50, January 2020. doi: 10.1051/0004-6361/201936588.

Joshua N. Winn and Daniel C. Fabrycky. The occurrence and architecture of exoplanetary systems. *Annual Review of Astronomy and Astrophysics*, 53(1):409–447, August 2015. ISSN 1545-4282. doi: 10.1146/annurev-astro-082214-122246. URL http://dx.doi.org/10.1146/annurev-astro-082214-122246.